Received: 6 August 2022 | Revised: 26 October 2022 | Accepted: 2 November 2022

DOI: 10.1111/ffe.13893

ORIGINAL ARTICLE

FFEMS Fatigue & Fracture of Engineering Materials & Structures WILEY

Data-driven approach to design fatigue-resistant notched structures

Qingbo Wang | **Chao Gao** | **Filippo Berto**

Department of Mechanical and Industrial Engineering, Norwegian University of Science and Technology, Trondheim, Norway

Correspondence
Qingbo Wang, Department of Mechanical and Industrial Engineering, Norwegian University of Science and Technology, Trondheim 7491, Norway.
Email: qingbo.wang@ntnu.no

Abstract

Fatigue is the most common failure mode for engineering materials in various industrial applications. Generally, designing new products and components based on typical deterministic fatigue design approaches is slow and expensive. Although numerous investigations have been carried on this topic over decades, there still lacks a robust and efficient method to design a super-fatigue-resistant and testless structure. In this investigation, a novel data-driven approach based on the deep learning algorithm is applied on designing a fatigue-resistant notched structure under different loading via numerical simulations and deep learning. The notches with various shapes are designed by employing the same material. Then finite element (FE) simulations are performed to obtain the mechanical behaviors of notched structures under different loading conditions. The deep learning algorithm is applied to predict mechanical behaviors of unknown notched structures based on input training set of simple notched geometries and relative lower computational cost. It is demonstrated that deep learning on the fatigue-resistant structure is a promising approach of fatigue design. This work offers an alternative design strategy of fatigue-resistant structure and cost-effective solution to accelerate the design of engineering components under different loading conditions.

KEYWORDS

data-driven approach, deep learning, fatigue-resistant, numerical simulation

1 | INTRODUCTION

Notched features such as holes, fillets, shoulders, grooves, and welded joints are widely present in structural components, and this geometric discontinuity can cause localized stress concentration at the notches during the structural loading process, which in turn initiates fatigue cracks.[1] The initiation and propagation of cracks lead to a reduction in the fatigue life of the structure under cyclic loading. Compared with cracks and sharp V-notches, blunt V-notches and U-notches are usually chosen as transition parts in structures because they are more effective in reducing stress concentration to achieve higher fatigue life. However, due to the fatigue size effect,[2] the fatigue life of notches is limited by notch opening angle, notch radius, and notch depth. The influence of size effect on fatigue has been evaluated through some experimental and numerical studies; for instance, critical distance theories and stress gradient were applied to predict fatigue life of samples with different depths and root

radii.[3–5] The relationship between fatigue life and fatigue region can be well described by correlating with the notch depth based on stress field intensity approach.[6] With the aim to study the effects of notch size on the fracture behavior of the specimens, different hole radii were analyzed through finite fracture mechanics theory.[7] The strain energy density (SED) was utilized to analyze the influence of notch radius and opening angles on fatigue life.[8–10] Although the fatigue assessment approaches mentioned above have been devoted to providing some unified methods for assessing the fatigue limit of notch features, they are all based on commonly utilized notches containing simple constituents, such as crack, V-notch, U-notch, and holes. The higher fatigue resistance of structures with notch components is limited by the notch shape design method, and there is still a lack of notch design approach that can be widely used and significantly improve the notch fatigue resistance.

In our previous work, a biomimetic fatigue design concept has been proposed to reveal that local topology of the structure can enhance the fatigue resistance.[11] The core concept is that materials cannot be immune from fatigue, but structures can. Filippo demonstrated that a variable radius notched joint has higher fatigue resistance than a commonly used constant edge radius specimen. The nonconstant radii notch consists of several separated curves, and the shape of which is related to the number of consisting curves and their corresponding radii. There does not exist, and also it is hard to build a theoretical fatigue assessment solution for nonconstant radii notched structures. Therefore, energy-based approach for fatigue assessment is still a good option. The SED is an advanced approaches for fatigue life assessment of notched structures under static conditions and fatigue failure.[12,13] The one main advantage of SED is that the method can use coarse mesh quality in FE simulations to identify the structural topology changes according to the critical volume in the notch vicinity.[14,15] In addition, the SED method is suitable for the application of different materials[16] and structures[17] under low cycle fatigue,[18] high cycle fatigue,[19] low temperature,[20] high temperature,[19] uniaxial[21] and mixed conditions,[22] which fully demonstrate the wide applicability and high performance of the SED method. However, the number of nonconstant notches generated in the design space is astronomical, and the SED fatigue assessment based on FE simulations quickly reaches its computational limits. In addition to the drawback of being computationally expensive and time-consuming, this computational simulation method is always related to limited design space and loading conditions, which makes it difficult to be generalized.

As a prevalent data-driven approach, deep learning has caught increasing attention in recent years. It has been widely applied to many fields, such as computer vision, natural language processing, and fault diagnosis, and remarkable success has been reported.[23–25] Compared with traditional methods, deep learning offers the benefits of simplifying the computational process and generalizing the application fields with less exhaustive algorithms and sensitive parameters in structure design. It explores the implicit relationship between the input and its target through the back-propagation algorithm and multi-layer hidden neurons. The aim of deep learning is to automatically build implicit patterns in complex data, which can be applied to predict unknown data. The major advantage of deep learning is that no significant human intervention or prior knowledge of the system is required. Therefore, it can automatically learn the relationships relative to the input design space and, thus, be generalized to different systems such as pattern recognition,[26,27] system health management and monitoring,[28,29] design for additive manufacturing,[30] and mechanical properties' prediction of complex structures and materials.[31,32]

The present paper is devoted to proposing an effective methodology to enhance the fatigue resistance of notched components. The main contributions of this work are summarized as follows:

1. A novel notched structure design method was proposed according to the stress concentration phenomenon and a biomimetic fatigue design concept, which provided a universal design idea regarding different notch features and in wide application spaces.
2. The convolutional neural network (CNN) was utilized to build the relationship between designed novel nonconstant notched structures with SED. In addition, this relationship is able to predict the SED of unknown notches and feedback the notch fatigue resistance optimization.
3. The comparison with commonly used blunt V-notch and U-notch exhibits the designed nonconstant notches have higher fatigue resistance.

The rest of this paper are organized as follows: The methods used in this work are detailed in Section 2. The simulation process and results are presented and discussed in Section 3. Finally, the conclusions of this work are summarized in Section 4.

2 | METHODS

2.1 | Notched structure design

Most structural components contain notch features such as holes, fillets, shoulders, grooves, and welded joints.

These materials' defects and geometrical discontinuities are the most loaded and dangerous places under working loadings,[1] which is also denoted as "stress concentrators"; that is, the greatest strains and stresses always occur in or around these places, which can lead to the initiation and propagation of fatigue cracks.[33] In order to reduce the stress concentration caused by geometric discontinuity, most of the optimized design notched structures are introduced with transition sections, such as the U-notch and blunt V-notch.[34–36] However, these notches are based on the constant radius, and the notch tip curvature or radius is the key parameter to governing the stress concentration and failure. The higher fatigue resistance of notched structures is limited by these empirically-based notch design methods. Currently, there is still no notch design concept that has been tested in practice and can be widely applied in fatigue resistance area.

However, some natural structures have been discovered with practically fatigueless.[11] For example, the joint between the peduncle and receptacle in sunflowers shows excellent fatigue resistance under cyclic wind loading conditions owing to the non-constant radius of curvature. Inspired by this fatigueless natural structure, a mathematical method is utilized to design the shape of notch with nonconstant radii in this paper, since the changes in radii inside the notch will cause local geometric discontinuity and, thus, generate stress concentration. We proposed that this stress concentration can be prevented through several connected arcs that tangent to each other. The tangent effect between the two arcs can be achieved by moving the center of the second arc to the extension of the radius of the first arc and sharing a part of the radius. The shape of the notch geometry consisting of these smoothly connected arcs can be changed by adjusting the position of the center of these arcs.

As shown in Figure 1A, the curve of the designed notch contains several small arcs, and the adjacent arcs share one part of the radius which is the way to keep arcs tangent to each other. It is worth noting that the design space does not have the limitation of units and the design approach can be applied to any scale of macrostructure and microstructure. In addition, another advantage of this method is its wide applicability, which is not limited by the manufacturing method. Both additive manufacturing and traditional manufacturing methods can customize the notches according to the design size. However, to facilitate analysis, the unit is set as 1 in this paper, and each arc occupies the same or the different units horizontally. Thus, the notch depth of the designed nonconstant notch is equal to the sum of units of all arcs in

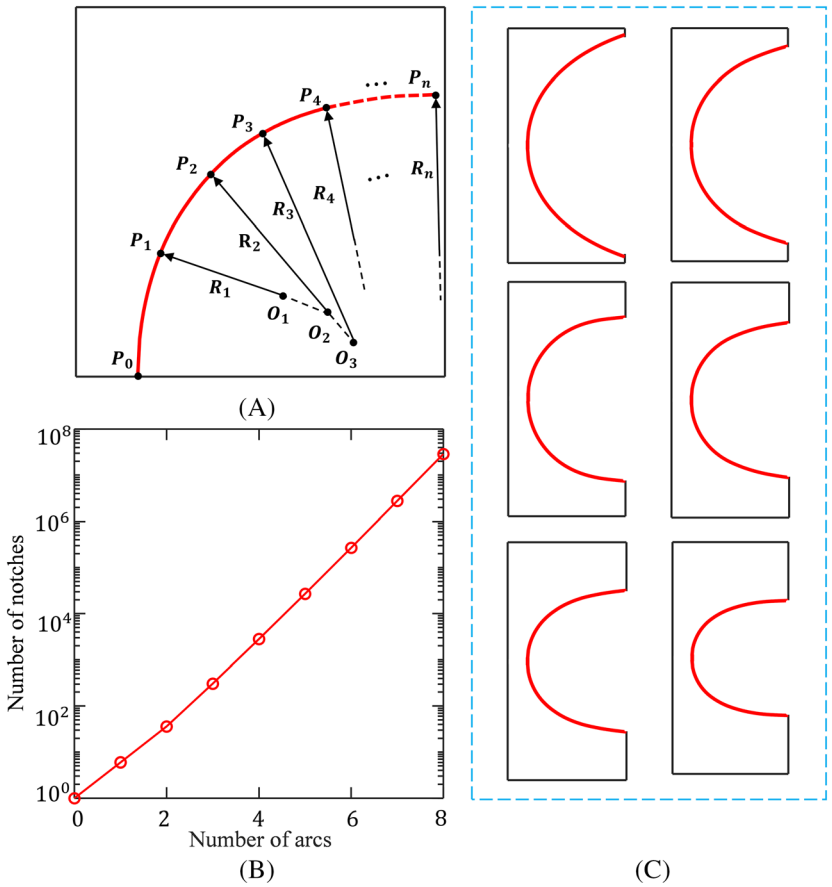

FIGURE 1 Nonconstant radii notch design: (A) design schematic, (B) the number of design notches, and (C) six designed nonconstant radii notches [Colour figure can be viewed at wileyonlinelibrary.com]

the horizontal direction. The center point, starting point, and ending point are the key information of each arc. And the ending point of the previous arc is the starting point of the latter arc. As a result, the position of the latter arc will change with the adjustment of the previous arc. Eventually, the shape of the designed nonconstant notch will also change. In Figure 1A, P_0, P_1, R_1, and O_1 are the starting point, the ending point, radius, and center of the first arc, respectively, in the Cartesian coordinate system. The starting point P_0 and the abscissa of the ending point P_1 are fixed. The abscissa of the center point O_1 is limited in the range of $(Ox_0 - Ox_1)$, and the Ordinate is also fixed. Then the Ordinate of the P_1 can be calculated based on the known information of the first arc. Finally, the Numel $(Ox_0 : a_1 : Ox_1)$ arcs are generated in the position of the first arc. The a_1 is the increment between Ox_0 and Ox_1, which is also a custom value. The generation of the second arc is based on the first arc. The center point O_2 of the second arc can be found on the extension of P_1 to O_1. In the meantime, the starting point of the second arc is the ending point P_1 of the first arc, and the abscissa of the ending point P_2 is fixed. After selecting the abscissa of the center of the second arc in the range $(Ox_1 : a_2 : Ox_2)$, the a_2 is similar to the custom value a_1, which is the increment between Ox_1 and Ox_2. The Ordinate of the center point and the ending point can be calculated through a straight-line equation and circle equation, respectively. The Numel$[(Ox_0 : a_1 : Ox_1) : a_2 : Ox_2]$ arcs are generated in the position of the second arc. Likewise, the other latter arcs can be generated in the same way. The number of custom-designed nonconstant notches is calculated in Equation (1).

$$N_n = numel\{[(Ox_0 : a_1 : Ox_1) : a_2 : Ox_2] : \cdots a_n : Ox_n\} \quad (1)$$

where N_n is the number of designed nonconstant notches consisting of n arcs. Ox_n is the abscissa of the center of the nth arc. a_n is the increment between Ox_n and the abscissa of the previous center.

In this work, for comparison with the most normally used U-notch and blunt V-notch, since they have similar shapes to our designed nonconstant notch, that is, consisting of an arc and a tangent line. Therefore, the design space is defined as a square, and its size is related to the number of consisting arcs. In the deep learning model, it is always difficult to find a "one size fits all" answer on how to determine the required minimum number of training data sets to construct the model, because the amount of the training data is dependent on many different aspects of the training process. Based on our preliminary study and parameters analysis of the deep learning model, tens of thousands of data are enough for training the deep learning model in this study. According to our notch design strategy, in the Cartesian coordinate system, when the starting point of the first arc is P_0 (2,0) and each arc occupied 2 units in the horizontal direction, as shown in Figure 1B, the number of notches is 27,056 when the notch consists of five arcs. When the notch is composed of six arcs, the number of notches can significantly increase to 269,710. Therefore, five arcs are chosen to generate the nonconstant notch, under the design space of 12*12. Figure 1C shows six designed nonconstant notches.

2.2 | Fatigue analysis approach

Brittle failure of components weakened by material defects and geometrical discontinuities is widely existing.[12] These crack-like defects can be simplified to sharp or blunt V-notches. According to the Williams' V-notch stress field theory, the stress levels at the tip of the notch can be characterized using notch stress intensity factors (NSIFs).[37,38] However, the calculation of NSIF requires the stresses near the notch tip. The notch tip stress needs a large amount of calculations because a very fine mesh is required in the FE simulations to obtain sufficient accuracy of the notch tip stress.[39]

In contrast to the NSIFs, the SED method does not require fine mesh quality. Due to its high performance in combining microcosmic phenomena and macrocosmic experimental evidence, the SED method has been demonstrated to use coarse mesh quality in FE simulations to identify the structural topology changes.[12] Moreover, the SED method is an energetic local approach, which has been proved as a method to investigate both fracture failure in static condition and fatigue failure.[15,40] The SED method is based on the knowledge that the structure failure occurs when the SED averaged over a given control volume reaches a critical value, $\overline{W} = W_C$. The W_C is related to the material itself. Therefore, it has the unique advantage to combine the energy-based criterion with the material-dependent structure.

In this work, various 2D designs of notched structure were compared in plane stress condition. Since the designed nonconstant notches have similar features (arc and the line or arcs tangent to it) with blunt V-notch and U-notch, therefore, the SED calculation of the nonconstant notches is referenced to the calculation of the blunt V-notch. The control volume is a crescent shape, and the R_0 is the maximum width as measured along the notch bisector line, as shown in Figure 2A.

$$R_0 = \frac{(5-3\nu)}{4\pi}\left(\frac{K_c}{\sigma_t}\right)^2 \quad (2)$$

where v represents the Poisson's ratio, K_C denotes fracture toughness, and σ_t is the ultimate tensile strength.

The SED $\overline{W}$ is expressed as

$$\overline{W} = H\left(2\alpha, \frac{R_0}{R}\right) \times \frac{K_{1\rho}^2}{E} \times \frac{1}{R^{2(1-\lambda_1)}} \tag{3}$$

where 2α denotes the opening angle, R represents the notch radius, and $H(2\alpha, R_0/R)$ depends on the previously defined parameters as listed in reference.[13] $K_{1\rho}$ is the notch stress intensity factor under mode 1, E stands for Young's modulus, and λ_1 stands for the Williams' eigenvalue.[13,41]

However, the designed notched structure in this work has nonconstant radii; as the result, the opening angle 2α and notch radius R both need to be modified according to the Equation (3). In order to represent the difference in the control volumes of all nonconstant radius notches, as shown in Figure 2B, the notch radius R is the radius of the first arc. The opening angle consists of a tangent line of the fifth arc that can avoid generating the same r_0.

2.3 | Data-driven approach

Here, the deep learning approach is served as the data-driven approach owing to its capability to establish a deep network architecture to discover the deep information embedded in huge data. The CNN model[42] is employed in this work. Inspired by the biological processes in that the neurons connected to the images are similar to the animal visual cortex, it is initially designed to analyze the visual imagery.[43–46] A typical CNN includes three building blocks: (1) convolutional layers, (2) pooling layers, and (3) fully connected layers. The procedure that transfers the input data through these pre-designed layers is known as forward propagation. The functionality of the layers is presented below.

2.3.1 | Convolutional layer

The convolution is the fundamental process in CNN, which is a specialized linear operation where the kernel overlays and slides through the entire input map with a pre-set stride. The stride represents a parameter of the kernel that defines the amount of movement over the input map. For each stride, the element-wise product between each element of the kernel and the overlaid input region is calculated and summed. Then, the summed output is fed into a nonlinear activation function. The final output of each stride forms a new feature map with a size smaller than input data. Extracted features are calculated as follows:

$$\boldsymbol{a}_k = Activ(b_k + \boldsymbol{Z}) \tag{4}$$

$$\boldsymbol{Z} = \sum_{i=1}^{inMap} Conv(\boldsymbol{W}_{ck}, \boldsymbol{X}_i) \tag{5}$$

where "*Activ*" and "*Conv*" represent the nonlinear activation function and the convolution process, respectively. $\boldsymbol{X}_i$ and $\boldsymbol{W}_{ck}$ are the input map and kernels, and b_k is the bias. The kernel is a randomly initialized small array of numbers that would be updated in the back propagation step. Generally, the convolution process can repeat with multiple kernels to generate more feature maps. Therefore, the subscript k defines the number of kernels as well as the output maps of this convolutional layer and the input maps of the next layer. $\boldsymbol{a}_k$ stands for the final extracted feature map.

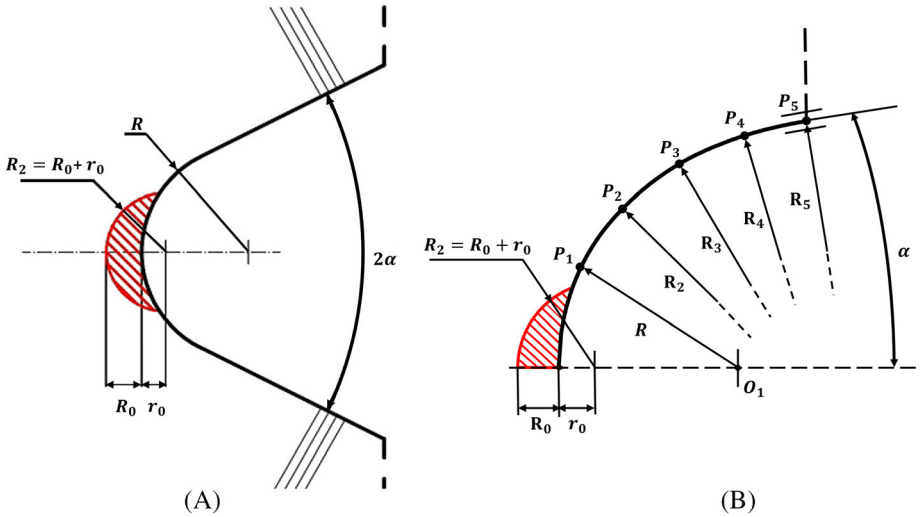

FIGURE 2 Critical volume (red area) for (A) blunt V-notch[12,17] and (B) nonconstant radii notch. Distance $r_0 = R \times (\pi - 2\alpha)/(2\pi - 2\alpha)$ [Colour figure can be viewed at wileyonlinelibrary.com]

2.3.2 | Pooling layer

The pooling layer is also called the subsampling layer; it is usually placed next to the convolutional layer. The pooling process represents a special type of the convolution process whereby the kernel slides through the entire input map, and instead of doing element-wise product, the maximum element or the average value of the overlaid input region is extracted; this quantity is the so-called "max pooling" or "average pooling," respectively. The pooling layer is used to merge similar features to reduce the number of parameters and achieve translation-invariant characteristics. The stride of the kernel in the pooling layer is usually equal to the size of the kernel.

2.3.3 | Fully connected layer

The main function of the fully connected layer is to merge the feature maps learned by different kernels. The convolutional layer and the pooling layer are stacked one by one. Finally, the extracted feature maps are to be flattened and concatenated into a vector at the fully connected layer. Let A denotes the concatenated feature vector. The output of last fully connected layer Y is given by

$$\boldsymbol{Y} = Activ\left(b + \boldsymbol{W}_f * \boldsymbol{A}\right) \tag{6}$$

where $\boldsymbol{A}$ = [flattened($\boldsymbol{a}_1$), flattened($\boldsymbol{a}_2$), ..., flattened ($\boldsymbol{a}_k$)] and $\boldsymbol{a}_k$ is the feature map of the last convolutional or pooling layer. $\boldsymbol{W}_f$ represents the weights that connect two layers of the neural network.

For the regression problems, the mean squared error (MSE) loss function is widely used in the form:

$$\boldsymbol{MSE} = \frac{1}{n}\sum_1^n \left(Y_i - \widehat{Y}_i\right)^2 \tag{7}$$

where n is the total number of data points and Y_i and $\widehat{Y}_i$ are actual and predicted values, respectively. The loss function aims at reducing the discrepancy between Y_i and $\widehat{Y}_i$.

3 | SIMULATIONS

3.1 | FE modeling and data generation

According to the notches design method of nonconstant notched structure, 27,056 different notches were generated in total in the initially given 12*12 design space, and each notch consists of five connected and tangent curves. Meanwhile, to compare the difference between generated notches, the depth of all notches was kept the same as 10.

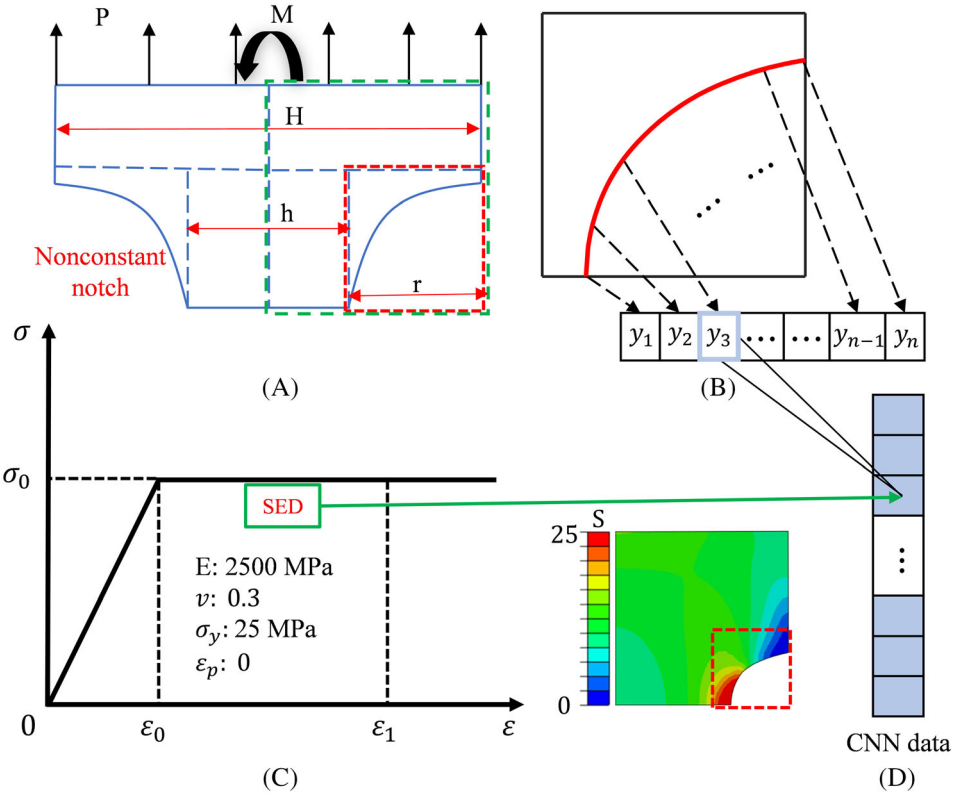

FIGURE 3 Simulation processes: (A) notched structure under tension and bending conditions, (B) generation of geometric data, (C) elastic-perfectly plastic material model with contour plot of Mises stress, and (D) CNN data preparation which contains geometric data and SED values [Colour figure can be viewed at wileyonlinelibrary.com]

Since the notches are important parts of structure, the designed nonconstant notches were considered as part of a structure in Figure 3A. According to the definition of the notched components in FKM-Guideline,[47] the ratio of the width of plate to the net width of a plate was set as 1.5, and the ratio of radius to net width of plate was set as 0.25. The radius is the notch depth and equals 10. Figure 3B presents the geometrical information of nonconstant notch. This illustrates the process of converting the curve information into a one-dimensional vector.

The FE modeling was utilized to obtain the SED, and the calculation processes were implemented in the commercial software ABAQUS 2019. The elastic-perfectly plastic material model was exploited in simulations. As shown in Figure 3C and Equation (8), the SED is equal to the area under the stress–strain diagram, which can be easily calculated in the elastic-perfectly plastic material model with 1 unit thickness and compared with different notched structures. Since there is no permanent deformation in the elastic-perfectly plastic model when material is unloaded, no energy is dissipated in the form of heat during simulations. Therefore, the SED can be utilized to measure the differences between notched structures.

$$\overline{W} = \int_0^{\varepsilon_1} \sigma_x d\varepsilon_x \tag{8}$$

where $\overline{W}$ represents the SED, $\sigma_x = \sigma_0$ is yield stress, and ε_x is measured from 0 to ε_1. FE simulations were performed in 2D plane stress condition under three different loading conditions-uniaxial tension, in-plane bending and out-of-plane bending. (1) Uniaxial tension. To reduce the computational cost, uniform pressure along y direction was applied on the quarter geometry with symmetry boundary condition along x and y directions, as shown in Figure 4. (2) In-plane bending. The bending moment under xy plane was applied on the half geometry with symmetry boundary condition along x direction. (3) Out-of-plane bending. The bending moment under yz plane was also applied on the half geometry with symmetry boundary condition along x direction. To ensure the load processes reaches the perfectly plastic part in the elastic-perfectly plastic material model, the applied loads under three loading conditions are selected and shown in Table 1. Moreover, the SED increased to the maximum after the last increment in every single simulation. The maximum SED values of all simulations were collected as the data set for CNN, as shown in Figure 3D. The data set also contains the geometrical information of all notches.

3.2 | CNN implementation details

3.2.1 | CNN structure and parameters optimization

A CNN architecture based on the AlexNet was constructed to solve the regression problems. As shown in Figure 5, AlexNet is a classic CNN architecture that is generally consisted of five convolutional layers with Sigmoid activation function, three average pooling layers, and one fully connected layer. The first convolutional layer adopted 16 filters with the size of 7, and the stride and padding size were set as 1 and 3, respectively. An average polling layer is attached at the end of the first convolutional layer with the size of 5 and the stride of 2. Likewise, the second convolutional layer used 32 filters with the size of 3 and the stride of 1, which is also

TABLE 1 Load in three loading conditions

Loading conditions	Load
Uniaxial tension	10 MPa (Pressure)
In-plane bending	5000 N.mm (Moment)
Out-of-plane bending	125 N.mm (Moment)

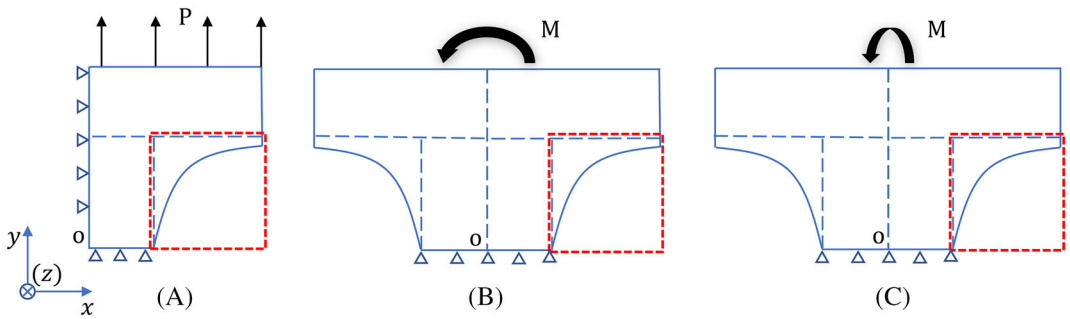

FIGURE 4 Three loading conditions: (A) uniaxial tension condition, (B) in plane bending condition, and (C) out of plane bending condition [Colour figure can be viewed at wileyonlinelibrary.com]

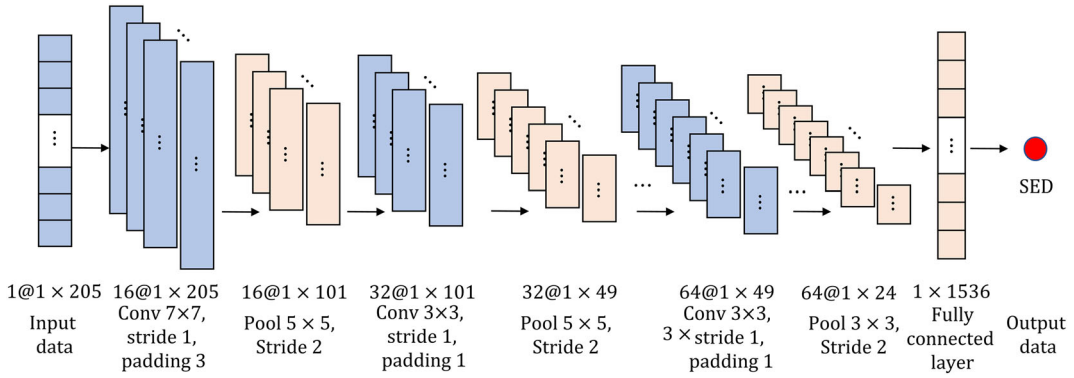

FIGURE 5 Architecture of CNN model [Colour figure can be viewed at wileyonlinelibrary.com]

followed by an average polling layer with the size of 5 and the stride of 2. Then, three stacked convolutional layers with the same 64 filters were used to extract the deeper information from input data, the filters size are 3, and the stride and the padding are both 1. The last average pooling layer with the size of 3 and the stride of 2 was used to downsize the extracted feature from upper layers. Finally, the extracted features were concatenated by the fully connected layers, which was fed into the final regression layer for prediction.

It is well-known that the hyperparameters of neural network directly impact the training process and model performance. Thus, it is crucial to adjust the hyperparameters that fit specific data sets with best performance. The learning rate is one of the most important parameters which controls how much the network weights are adjusted according to the loss gradient. To increase the model learning efficiency and avoid suboptimal solution, an adaptive learning rate method called Adam stochastic optimization algorithm is applied to update the network weights with the learning rate of 0.0001; the mathematical details are expressed as follows:

$$m_t = \beta_1 m_{t-1} + (1-\beta_1) g_t \tag{9}$$

$$v_t = \beta_2 v_{t-1} + (1-\beta_2) g_t^2 \tag{10}$$

$$\widehat{m_t} = \frac{m_t}{1-\beta_1^t} \tag{11}$$

$$\widehat{v_t} = \frac{v_t}{1-\beta_2^t} \tag{12}$$

where m_t and v_t represent the estimates of the first moment and the second moment of the gradients, respectively (both are initialized as zero); β_1 and β_2 are decay rates, and usually set as 0.9 and 0.99; $\widehat{m_t}$ and $\widehat{v_t}$ are bias-corrected first and second moment estimates. The parameter is updated using the following equation.

$$\theta_{t+1} = \theta_t - \frac{lr}{\sqrt{\widehat{v_t}} + \epsilon} \widehat{m_t} \tag{13}$$

where θ stands for the network weights, and lr represents the learning rate.

3.2.2 | Fatigue-resistance notch structure prediction

To analyze the effect of training parameters from the CNN model on the prediction accuracy, the SED was used to evaluate the regression performance; that is, all calculated SED values by FE simulations were considered as the ground truth. The training data-to-entire data set ratio is a crucial factor that effects the model performance. Therefore, the influence of training data-to-entire data set ratio on prediction accuracy was investigated. Different training data sets were chosen from the generated whole 27,056 one-dimensional data set, and the remaining was considered as testing data. Prediction accuracies of the CNN model as a function of the different ratios of training data ranging from 10% to 90% are shown in Figure 6A. Other parameters remained unchanged. At the beginning of the experiment, the SED value matrices of training data and testing data were normalized using the "z-score" method, a variation of scaling that represents the number of standard deviations away from the mean, which transforms features to be on a similar scale to improve the performance and training stability of the model. In addition, the prediction threshold was set to be 1% of the normalization interval. Figure 6A shows that as training data ratio increases, the prediction accuracy increases up to over 99%. The results show that

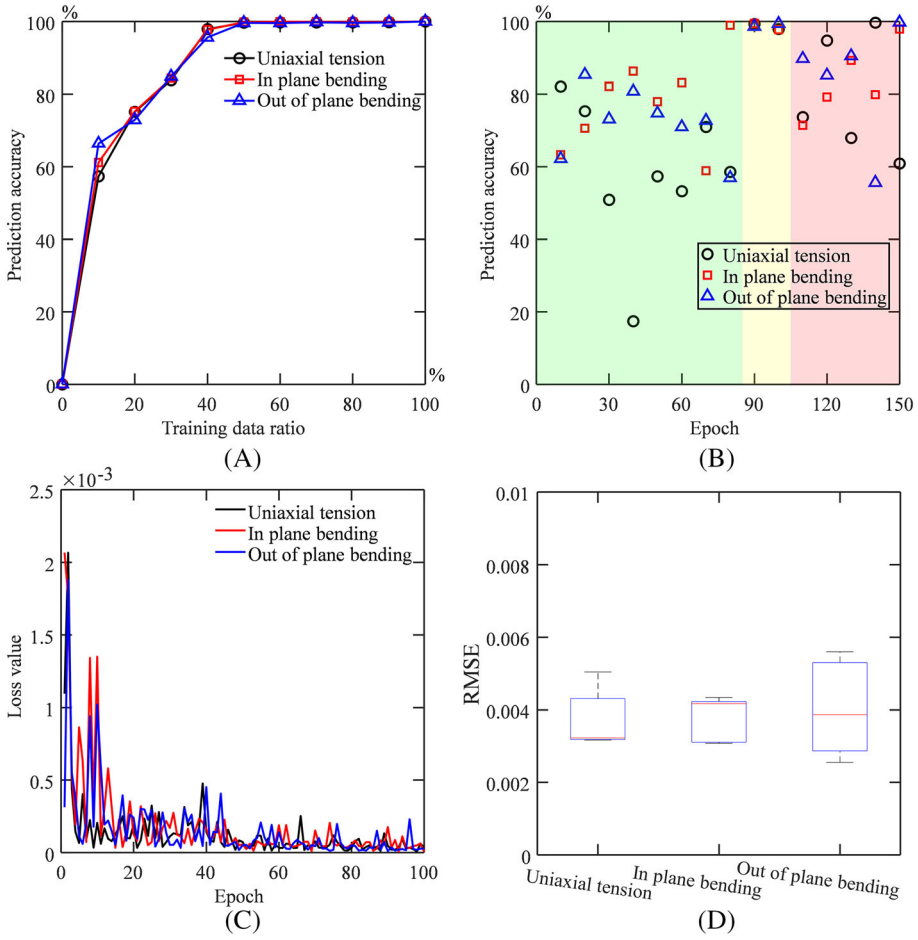

FIGURE 6 Training parameters optimization of CNN model: (A) prediction accuracy as a function of the training data ratio, (B) prediction accuracy as a function of the number of epochs, (C) evolution of loss value in training process of CNN, and (D) RMSE of prediction results [Colour figure can be viewed at wileyonlinelibrary.com]

CNN model can achieve very high prediction performance and the prediction accuracy was already higher than 95% when 40% of data (10,800 data points) was selected to train the CNN model.

Moreover, the influence on prediction accuracy of the number of epochs was investigated. An epoch in the CNN model means one complete pass of the training dataset through the algorithm. The number of epochs is an important hyperparameter for the CNN model, generally, increasing the number of epochs can improve the model performance on training dataset, but in the meantime, consume more computational cost, and sometimes, even lead to overfitting problem on testing dataset. Therefore, a suitable number of epochs can guarantee high model training efficiency and performance. According to the training data ratio analysis experiment, the CNN model already could achieve high prediction accuracy with around 10,000 data. Therefore, to balance the training performance and computational cost, random 10,800 data were selected in the whole data set to quantify the number of epochs. The CNN model was trained with a number of epochs ranging from 10 to 150. As shown in Figure 6B, the CNN model has high prediction accuracy and efficiency when the epoch number was set as 100 in three loading conditions.

The loss value of training process was shown in Figure 6C, as one can see, the loss value gradually converges to zero with the increase of the number of epochs. The root mean square error (RMSE) is a measure for evaluating the prediction quality through the error between predicted value and true value. RMSE of prediction results are shown in Figure 6D. RMSE is very small under the three loading conditions, which means the predicted SED values are close to the real SED value.

Finally, the optimized training parameters are selected based on the above experiments. The regression performance of the CNN model is shown through the comparison between true SED values and predicted SED values. The distributions of the randomly selected 10,800 normalized SED values during training process of the CNN model in each of the three loading conditions are shown in Figure 7A. And the distribution is also demonstrated to be relevant to the notch design strategy. Most SED values are in the right half of the distribution range, which correspond to lower fatigue life. The rest 16,200 SED values are ground truth for verifying the predicted

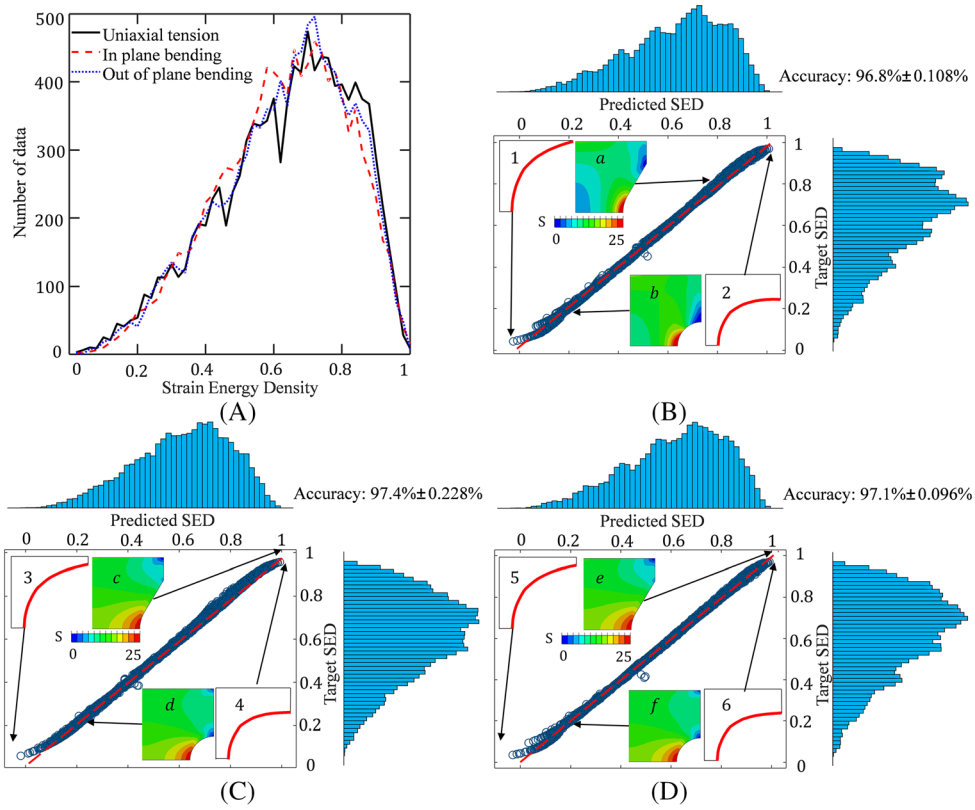

FIGURE 7 Training data distributions, predicted results of CNN model, and contour plot of Mises stress of blunt V-notch and U-notch: (A) SED distributions of uniaxial tension, in plane bending and out of plane bending, (B) CNN prediction of uniaxial tension condition, (C) CNN prediction of in plane bending condition, and (D) CNN prediction of out of plane bending condition [Colour figure can be viewed at wileyonlinelibrary.com]

performance of the CNN model under three loading conditions separately. The SED values of the corresponding testing nonconstant notched geometries were predicted through the trained CNN model. Then the predicted SED values against true SED values are shown in Figure 7B–D. One can see that they all show similar distribution to training data. The X-axis and Y-axis represent the predicted and true SED values, respectively, in Figure 7B–D. If the predicted SED values are the same as the true SED values, the scatter points shall locate exactly on the red dotted diagonal line. Therefore, the closer the prediction is to the true SED value, the closer the scatter is to the diagonal line. It can be seen that when the threshold is set to 1% of the data range size, the prediction accuracies are all higher than 95%. And the prediction accuracies under the three loading conditions are around 96.8%, 97.4%, and 97.1%, respectively.

Since each predicted SED value is related to a designed nonconstant notched geometry, and according to the fatigue data in terms of SED value,[13] the lower SED value is corresponding to the higher fatigue resistance. Hence, the desired fatigue-resistant notched structure could be selected according to the SED value. And the superiority of the nonconstant notched geometry design approach and deep learning method can be demonstrated by comparing with conventional notches. As shown in Figure 7B, the nonconstant notched geometries "1" and "2" are corresponding to the lowest and highest SED values in the uniaxial tension condition. The SED values of commonly utilized blunt V-notch "a" (the arc part has same radius as the first arc in "1" geometry) and U-notch "b" (it has the biggest radius in design space) are both higher than the SED value of geometry "1." Likewise, geometries "3" and "5" also have the smallest SED values for their respective loading conditions in Figure 7C,D.

4 | CONCLUSION AND FUTURE WORK

In this paper, the CNN was applied to predict the SED value of notched structure and identify the fatigue resistance of nonconstant notched structure in a generalized design space. First, a novel nonconstant notched geometry design approach was proposed, and it can be applied to design spaces of different sizes and fully avoid local stress concentration. Then, the SED, which does not require very refined mesh in the FE modeling process, was utilized to measure the fatigue resistance of notched structure. Finally, The CNN model was adopted to predict the SED values. The FE simulations results have shown that the CNN model is able to achieve high prediction accuracy, and the designed nonconstant notched structure has higher fatigue resistance than conventional notches.

Future work includes applying this fatigue resistance notched structure design approach to complex mixed

loading conditions and validating the designed structures through the additive manufacturing and fatigue tests. In addition, the method can be expanded to assist in the local and global fatigue resistance design and optimization of components containing notch features such as holes, fillets, shoulders, grooves, and welded joints.

CONFLICT OF INTEREST

The authors declare that they have no known competing financial interests or personal relationships that could have appeared to influence the work reported in this paper.

AUTHOR CONTRIBUTIONS

Qingbo Wang: Conceptualization; methodology; software; validation; formal analysis; writing-original draft; visualization. **Chao Gao:** Conceptualization; writing-review and editing; supervision. **Filippo Berto:** Conceptualization; supervision.

DATA AVAILABILITY STATEMENT

The data that support the findings of this study are available from the corresponding author upon reasonable request.

ORCID

Qingbo Wang https://orcid.org/0000-0002-0923-8643
Chao Gao https://orcid.org/0000-0003-4023-0970

REFERENCES

1. Liao D, Zhu S-P, Correia JAFO, De Jesus AMP, Berto F. Recent advances on notch effects in metal fatigue: a review. *Fatigue Fract Eng Mater Struct*. 2020;43(4):637-659.
2. Tridello A, Niutta CB, Berto F, Paolino DS. Size-effect in very high cycle fatigue: a review. *Int J Fatigue*. 2021;153:106462.
3. Sangsefidi M, Akbardoost J, Zhaleh AR. Assessment of mode I fracture of rock-type sharp V-notched samples considering the size effect. *Theor Appl Fract Mech*. 2021;116:103136.
4. Santus C, Berto F, Pedranz M, Benedetti M. Mode III critical distance determination with optimized V-notched specimen under torsional fatigue and size effects on the inverse search probability distribution. *Int J Fatigue*. 2021;151:106351.
5. Morgan D, Quinlan S, Taylor D. Using the theory of critical distances to predict notch effects in fibre composites. *Theor Appl Fract Mech*. 2022;118:103285.
6. Wu Y-L, Zhu S-P, He J-C, Liao D, Wang Q. Assessment of notch fatigue and size effect using stress field intensity approach. *Int J Fatigue*. 2021;149:106279.
7. Torabi AR, Etesam S, Sapora A, Cornetti P. Size effects on brittle fracture of Brazilian disk samples containing a circular hole. *Eng Fract Mech*. 2017;186:496-503.
8. Song W, Liu X, Yan D. Notch size effect on in-phase multiaxial fatigue life prediction of steel bar specimens. *Mater Des Process Commun*. 2019;1(3):e54.
9. Justo J, Castro J, Cicero S. Energy-based approach for fracture assessment of several rocks containing U-shaped notches through the application of the SED criterion. *Int J Rock Mech min Sci*. 2018;110:306-315.
10. Negru R, Serban DA, Pop C, Marsavina L. Notch effect assessment in a PUR material using a ring shaped specimen. *Theor Appl Fract Mech*. 2018;97:500-506.
11. Berto F, Razavi J. Fatigueless structures inspired by nature: a case study. *Mater Des Process Commun*. 2019;1(3):e27.
12. Berto F. Fatigue and fracture assessment of notched components by means of the strain energy density. *Eng Fract Mech*. 2016;167:176-187.
13. Berto F, Lazzarin P. Recent developments in brittle and quasi-brittle failure assessment of engineering materials by means of local approaches. *Mater Sci Eng R Rep*. 2014;75:1-48.
14. Lazzarin P, Berto F, Zappalorto M. Rapid calculations of notch stress intensity factors based on averaged strain energy density from coarse meshes: theoretical bases and applications. *Int J Fatigue*. 2010;32(10):1559-1567.
15. Berto F. A criterion based on the local strain energy density for the fracture assessment of cracked and V-notched components made of incompressible hyperelastic materials. *Theor Appl Fract Mech*. 2015;76:17-26.
16. Campagnolo A, Meneghetti G, Berto F, Tanaka K. Crack initiation life in notched steel bars under torsional fatigue: synthesis based on the averaged strain energy density approach. *Int J Fatigue*. 2017;100:563-574.
17. Foti P, Berto F. Fatigue assessment of high strength welded joints through the strain energy density method. *Fatigue Fract Eng Mater Struct*. 2020;43(11):2694-2702.
18. Zhao P, Lu T-Y, Gong J-G, Xuan F-Z, Berto F. A strain energy density based life prediction model for notched components in low cycle fatigue regime. *Int J Press Vessels pip*. 2021;193:104458.
19. Gallo P, Berto F. Advanced materials for applications at high temperature: fatigue assessment by means of local strain energy density. *Adv Eng Mater*. 2016;18(12):2010-2017.
20. Viespoli LM, Leonardi A, Cianetti F, Nyhus B, Alvaro A, Berto F. Low-temperature fatigue life properties of aluminum butt weldments by the means of the local strain energy density approach. *Mater Des Process Commun*. 2019;1(1):e30.
21. Kusch A, Salamina S, Crivelli D, Berto F. Strain energy density as failure criterion for quasi-static uni-axial tensile loading. *Frat Integrita Strutt*. 2021;15(57):331-349.
22. Razavi SMJ, Aliha MRM, Berto F. Application of an average strain energy density criterion to obtain the mixed mode fracture load of granite rock tested with the cracked asymmetric four-point bend specimens. *Theor Appl Fract Mech*. 2018;97:419-425.
23. Hassaballah M, Awad AI. *Deep Learning in Computer Vision: Principles and Applications*. CRC Press; 2020.
24. Otter DW, Medina JR, Kalita JK. A survey of the usages of deep learning for natural language processing. *IEEE Trans Neural Netw Learn Syst*. 2020;32(2):604-624.
25. Hoang D-T, Kang H-J. A survey on deep learning based bearing fault diagnosis. *Neurocomputing*. 2019;335:327-335.
26. LeCun Y, Bengio Y, Hinton G. Deep learning. *Nature*. 2015;521(7553):436-444.
27. Chen X-W, Lin X. Big data deep learning: challenges and perspectives. *IEEE Access*. 2014;2:514-525.

28. Khan S, Yairi T. A review on the application of deep learning in system health management. *Mech Syst Signal Process*. 2018; 107:241-265.
29. Azimi M, Eslamlou AD, Pekcan G. Data-driven structural health monitoring and damage detection through deep learning: state-of-the-art review. *Sensors*. 2020;20(10):2778.
30. Després N, Cyr E, Setoodeh P, Mohammadi M. Deep learning and design for additive manufacturing: a framework for microlattice architecture. *Jom*. 2020;72(6):2408-2418.
31. Yang Z, Yu C-H, Buehler MJ. Deep learning model to predict complex stress and strain fields in hierarchical composites. *Sci Adv*. 2021;7(15):eabd7416.
32. Maurizi M, Gao C, Berto F. Interlocking mechanism design based on deep-learning methods. *App Eng Sci*. 2021;7:100056.
33. Biłous P, Łagoda T. Structural notch effect in steel welded joints. *Mater Des*. 2009;30(10):4562-4564.
34. Shen W, Qiu Y, Hu Y, Liu E, Pan J. A simplified method for evaluating singular stress field of V-shaped and U-shaped notches with different opening angle. *Ocean Eng*. 2020;210: 107352.
35. Hobbacher A. *Recommendations for Fatigue Design of Welded Joints and Components*. Vol. 47. Springer; 2016.
36. Liu W, Yao X, Ma Y, Chen X, Guo G, Ma L. Prediction on fatigue life of U-notched PMMA plate. *Fatigue Fract Eng Mater Struct*. 2017;40(2):300-312.
37. Savruk MP, Kazberuk A. *Stress Concentration at Notches*. Springer; 2017.
38. Radaj D. State-of-the-art review on extended stress intensity factor concepts. *Fatigue Fract Eng Mater Struct*. 2014;37(1): 1-28.
39. Luo P, Zhang Q, Bao Y, Zhou A. Fatigue evaluation of rib-to-deck welded joint using averaged strain energy density method. *Eng Struct*. 2018;177:682-694.
40. Braun M, Fischer C, Fricke W, Ehlers S. Extension of the strain energy density method for fatigue assessment of welded joints to sub-zero temperatures. *Fatigue Fract Eng Mater Struct*. 2020; 43(12):2867-2882.
41. Williams M. Stress singularities resulting from various boundary conditions in angular corners of plates in extension. *J Appl Mech*. 1952;19(4):526-528.
42. Yamashita R, Nishio M, Do RKG, Togashi K. Convolutional neural networks: an overview and application in radiology. *Insights Imaging*. 2018;9(4):611-629.
43. Yang C, Kim Y, Ryu S, Gu GX. Prediction of composite microstructure stress-strain curves using convolutional neural networks. *Mater Des*. 2020;189:108509.
44. Gu GX, Chen C-T, Buehler MJ. De novo composite design based on machine learning algorithm. *Extreme Mech Lett*. 2018; 18:19-28.
45. Pierson K, Rahman A, Spear AD. Predicting microstructure-sensitive fatigue-crack path in 3d using a machine learning framework. *Jom*. 2019;71(8):2680-2694.
46. Kantzos C, Lao J, Rollett A. Design of an interpretable convolutional neural network for stress concentration prediction in rough surfaces. *Mater Charact*. 2019;158:109961.
47. Lee Y-L, Barkey ME, Kang H-T. *Metal Fatigue Analysis Handbook: Practical Problem-Solving Techniques for Computer-Aided Engineering*. Elsevier; 2011.

How to cite this article: Wang Q, Gao C, Berto F. Data-driven approach to design fatigue-resistant notched structures. *Fatigue Fract Eng Mater Struct*. 2022;1-12. doi:10.1111/ffe.13893